PERGAMON

International Journal of Solids and Structures 39 (2002) 261–276

INTERNATIONAL JOURNAL OF SOLIDS and STRUCTURES

www.elsevier.com/locate/ijsolstr

A point assembly method for stress analysis for two-dimensional solids

G.R. Liu *

SMA Fellow, Singapore-MIT Alliance, Center for Advanced Computations in Engineering Science, Department of Mechanical Engineering, National University of Singapore, 10 Kent Ridge Crescent, S 119260, Singapore

Received 14 January 1999

Abstract

A novel point assembly method (PAM) is presented for stress analysis for two-dimensional solids. In the present method, the boundaries of the problem domain are represented by a set of discrete points, and the domain itself is represented by properly scattered points. The displacement in the influence triangular areas of a point is interpolated by the displacements at the point and pairs of surrounding points using shape functions. The shape functions used in this work are obtained in the same way as those of a triangular element in the conventional finite element method (FEM). A variational (weak) form of the equilibrium equation is used to produce a set of system equations. These equations are assembled for all the points in the domain, and solved for the displacement field. Stresses and strains at a point are then computed using the displacements obtained for the point and pairs of the surrounding points. A PAM program with an automatic point-searching algorithm has been developed in FORTRAN. Patch tests and convergence studies have been carried out to verify the convergence of the present method and program. Examples are also presented to demonstrate the efficiency and accuracy of the present method compared with analytical solutions as well as the conventional FEM solutions. © 2001 Published by Elsevier Science Ltd.

Keywords: Finite element method; Element free Galerkin method; Element free method; Meshless method; Mesh free method; Finite point method; Numerical analysis

1. Introduction

The finite element method (FEM) is robust, and thoroughly developed for static and dynamic, linear and non-linear stress analyses of solids and structures. It is widely used in engineering due to its versatility for solids and structures of complex geometry and its flexibility for many types of non-linear problems. However, limitations of the FEM are becoming evident gradually for problems related to the distortion of elements caused by extreme conditions such as high velocity impacts and explosion/shock loadings, and problems of simulating breakage and crack progressing in materials. A close examination of these problems

* Tel.: +65-874-6481; fax: +65-874-4795/779-1459.
E-mail address: mpeliugr@nus.edu.sg (G.R. Liu).
URL: http://www.nus.edu.sg/ACES/aces.htm.

0020-7683/01/$ - see front matter © 2001 Published by Elsevier Science Ltd.
PII: S0020-7683(01)00172-X

associated with the FEM will leads one's attention to the root of the problems: the use of "*element*", the building block of the FEM. As long as the element is used, the problems mentioned above will not have an easy solution. Therefore, the idea of getting rid of the elements has been naturally evolving. Concepts of element free or meshless methods have been proposed during the past years. The element free method (EFM) has great potential for solving difficult problems associated with element distortion. Adaptive schemes can be easily developed, as there is no element in the mesh. In crack growth problems, for example, nodes can be easily added around a crack tip to capture the stress concentration with a desired accuracy; this nodal refinement can be moved with a propagation crack through a background arrangement of nodes associated with the global geometry. Adaptive meshing for a large variety of problems, 2D or 3D, including linear and non-linear, static and dynamic stress analysis, can be very effectively treated in EFM in a relatively simple manner.

The present EFMs include the element free Galerkin (EFG) method (e.g., Belytschko et al., 1994a,b, 1995a,b, 1996a,b; Lu et al., 1994; Krysl et al., 1995; Liu and Yang, 1998), reproducing Kernel particle method (e.g., Liu and Chen, 1995; Liu et al., 1995a,b), hp-clouds (Duarte and Oden, 1995), diffuse element method (Nayroles et al., 1992), finite point method (Oqate et al., 1995, 1996), and smooth particle hydrodynamics (SPH) method (e.g., Gingold and Moraghan, 1977; Moraghan, 1982, 1988). Reviews and comparison studies of some of the above mentioned methods have been given by Belytschko et al. (1996a) and Oqate et al. (1996).

However, because the meshless methods are still in its infant stage, there exist following major technical problems for stress analysis for solids and structures:

1. Many methods need a background mesh for the integration in computing the stiffness matrix.
2. Difficulties in the implementation of essential boundary conditions.
3. Complexity in algorithms for computing the interpolation functions, which makes the methods expensive.

To overcome the first problem, a method has been proposed by Beissel and Belytschko (1996), which results in a completely meshless method. Shape functions in meshless methods are constructed using methods such as moving least squares (MLS) for all the points within the influence area of a point (or a Gauss integration point). Therefore the interpolants do not have the Kronecker delta property. This makes it difficult to impose essential boundary conditions. The method of Lagrange multiplier is used as a standard method to impose essential boundary conditions. The penalty method is an alternative means for enforcing the essential boundary condition (Liu and Yang, 1998). Approaches, such as using d'Alembert's principle and modified shape functions, have also been proposed (Liu et al., 1996; Gosz and Liu, 1996; Günther and Liu, 1998). The third problem is still remaining open, and a break through in this aspect can bring the meshless method to a new height.

This paper deals with these three problems. A point assembly method (PAM) is proposed as a possible solution to these problems. In the PAM, the boundaries of the problem domain are represented by a set of discrete points, and the domain itself is represented by properly scattered points. The influence area of a point consists of pieces of triangular areas formed by its surrounding points. The displacement in a triangular area surrounding a point is interpolated by the displacements at the point and a pair of consecutive surrounding points using shape functions. The shape functions used in the present work are obtained in the same way as those of a triangular element in the conventional FEM. Hence, the shape functions can be obtained very efficiently and have the Kronecker delta property. The essential boundary conditions can be simply imposed as it is done in the conventional FEM. Hence, the second and third problems are dealt with.

A variational (weak) form of the equilibrium equation is used to produce a set of system equations for the triangular areas surrounding a point. These equations are assembled for all the points in the domain, and hence the first problem is taken care of. Solving these equations for the displacement field, the stresses

and strains at a point are then computed using the displacements obtained for the point and pairs of the surrounding points.

A PAM program with an automatic point-searching algorithm has been developed in FORTRAN. Two dimensional problem is handled in this paper, as the purpose of this work is to present and examine the concept of the present PAM. Patch tests and convergence studies have been carried out to verify the convergence of the present method and program. Examples are also presented to demonstrate the efficiency and accuracy of the present method compared with analytical solutions as well as the conventional FEM solutions.

2. The concept of point assembly method

Two-dimensional problems are considered here to present the concept of the PAM. For a given problem domain shown in Fig. 1, a set of points are used to represent the boundary of the domain. The boundary points are arranged in the order of counter clockwise direction. The internal domain is marked with properly scattered internal points. The influence area of point A within a cycle of diameter d_g has the shape of a *palm*. The palm of point A consists of six triangles: ABC, ACD, ADE, AEF, AFG and AGB, which are separated by six ribs. The palm of point K consists of three triangles separated by two internal ribs and two ribs on the boundary. A palm can be formed for any given point. The displacement at any point within a palm can be interpolated using the displacements at three nodes of the triangle hosting this points using shape functions, which are being used in the conventional FEM. The stiffness of the triangles contributes to all the points covered by the palm. An assembly for all the points within the domain can then be performed to form a globe stiffness matrix. A set of globe system equations can be obtained and solved for the displacement at all the points. In retrieving the stress and strain at any point, a palm of the point can be formed again to compute the stresses and strains in the triangles in the palm. The stress and strain at the point can be obtained by averaging the stresses and strains in the triangles within the palm.

3. Formulation

The equilibrium equation at a point in a solid can be written the form of

$$\vec{\nabla} \cdot \boldsymbol{\sigma} + \mathbf{b} = 0 \quad \text{in } \Omega \tag{1}$$

where $\boldsymbol{\sigma} = \{\sigma_{xx}\ \sigma_{yy}\ \sigma_{xy}\}^{\mathrm{T}}$ is the stress and $\mathbf{b}$ is the body forces in the problem domain Ω. The boundary conditions for displacement $\mathbf{u} = \{u_x \quad u_y\}^{\mathrm{T}}$ and stress $\boldsymbol{\sigma}$ are given, respectively, by

$$\mathbf{u} = \bar{\mathbf{u}} \quad \text{on } \Gamma_{\mathrm{u}} \tag{2}$$

$$\mathbf{n} \cdot \boldsymbol{\sigma} = \bar{\mathbf{t}} \quad \text{on } \Gamma_{\mathrm{t}} \tag{3}$$

where $\bar{\mathbf{u}}$ and $\bar{\mathbf{t}}$ are, respectively, the prescribed displacement on the essential boundary Γ_{u} and traction on the natural boundary Γ_{t}, and $\mathbf{n}$ is the unit outward normal to the boundary of domain Ω. The functional, Π, is the potential energy given by

$$\Pi(\mathbf{u}) = \int_{\Omega} \left[\frac{1}{2}\boldsymbol{\varepsilon}(\mathbf{u}) : \boldsymbol{\sigma}(\mathbf{u}) - \mathbf{u} \cdot \mathbf{b}\right] \mathrm{d}\Omega - \int_{\Omega} \mathbf{u} \cdot \bar{\mathbf{t}}\, \mathrm{d}\Gamma \tag{4}$$

where $\mathbf{u}$ is an assumed displacement vector with C^0 continuity, and the strain $\boldsymbol{\varepsilon} = \{\varepsilon_{xx} \quad \varepsilon_{yy} \quad \varepsilon_{xy}\}^{\mathrm{T}}$ is obtained by

$$\boldsymbol{\varepsilon} = \mathbf{L}\mathbf{u}, \quad \boldsymbol{\sigma} = \mathbf{D}\boldsymbol{\varepsilon} \tag{5}$$

where the differential operator is given by

$$\mathbf{L}^{\mathrm{T}} = \begin{bmatrix} \frac{\partial}{\partial x} & 0 & \frac{\partial}{\partial y} \\ 0 & \frac{\partial}{\partial y} & \frac{\partial}{\partial x} \end{bmatrix} \tag{6}$$

The matrix **D** in Eq. (5) is a matrix of elastic constants. For isotropic material and plane stress problems, we have

$$\mathbf{D} = \frac{E}{1-v^2} \begin{bmatrix} 1 & v & 0 \\ v & 1 & 0 \\ 0 & 0 & (1-v)/2 \end{bmatrix} \tag{7}$$

where E and v are the Young's modulus and Poisson's ratio of the material. For an anisotropic material, **D** can be a full matrix.

Within a palm shown in Fig. 1, the displacement field can be given by

$$\mathbf{u} = \mathbf{N}(\mathbf{x})\mathbf{d} \tag{8}$$

where **N** is a matrix of shape functions. The formulae of these shape functions are the same as those of a triangle element of the conventional FEM which can be found in any text book on FEM (e.g., Zienkiewicz and Taylor, 1989). Vector **d** consists of the displacements at all the points covered by the palm (seven points for the palm of point A and five points for the palm of point K shown in Fig. 1).

Substituting the expression of **u** into the weak form Eq. (4) yields:

$$\mathbf{K}\mathbf{u} = \mathbf{f} \tag{9}$$

where **K** is the stiffness matrix given by

$$\mathbf{K} = \int_{\Omega} \mathbf{B}^{\mathrm{T}}\mathbf{D}\mathbf{B}\,\mathrm{d}\Omega \tag{10}$$

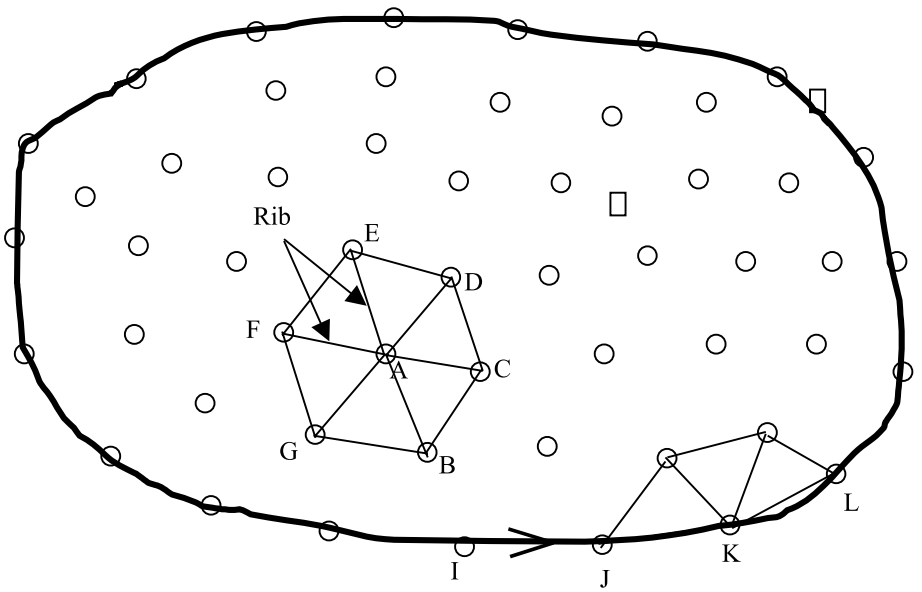

Fig. 1. Palm structures for point A and point K.

where

$$\mathbf{B} = \mathbf{L}\mathbf{N} \tag{11}$$

The force vector in Eq. (9) can be given in the form of

$$\mathbf{f} = \int_{\Gamma_t} \mathbf{N}\bar{\mathbf{t}}\,\mathrm{d}\Gamma + \int_{\Omega} \mathbf{N}\mathbf{b}\,\mathrm{d}\Omega \tag{12}$$

Eqs. (11) and (12) are integrated over the problem domain by a quadrature scheme which samples the integrand only at the points (Beissel and Belytschko, 1996). We can then obtain

$$\mathbf{K} \cong \sum_{I=1}^{N_p} \alpha_I^{\Omega} \mathbf{B}^{\mathrm{T}}(\mathbf{x}_I)\mathbf{D}(\mathbf{x}_I)\mathbf{B}(\mathbf{x}_I) \tag{13}$$

$$\mathbf{f} \cong \sum_{I=1}^{N_t} \alpha_I^{\Gamma_t} \mathbf{N}^{\mathrm{T}}(\mathbf{x}_I)\bar{\mathbf{t}}(\mathbf{x}_I) + \sum_{I=1}^{N_p} \alpha_I^{\Omega} \mathbf{N}^{\mathrm{T}}(\mathbf{x}_I)\mathbf{b}(\mathbf{x}_I) \tag{14}$$

where N_p is the total number of points in the problem domain, and N_t is number of the points on the natural boundary where traction is prescribed. Coefficients α_I^{Ω} and $\alpha_I^{\Gamma_u}$ are, respective, the fractions of the area and the length represented by point I. These coefficients are related to the ratio of area overlapping induced by the point assembly procedure. In this work, we define

$$\alpha_I^{\Omega} = \frac{A_I}{\sum_{i=1}^{N_p} A_i} A_{\Omega} \tag{15}$$

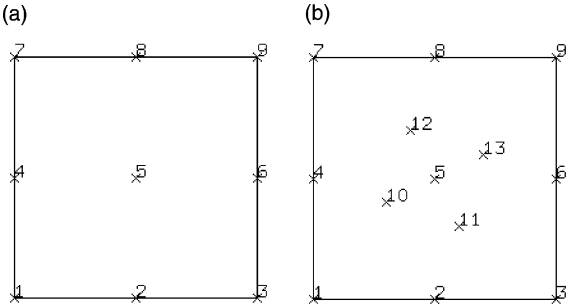

Fig. 2. Points configurations for patch tests: (a) patch test 1 and (b) patch test 2.

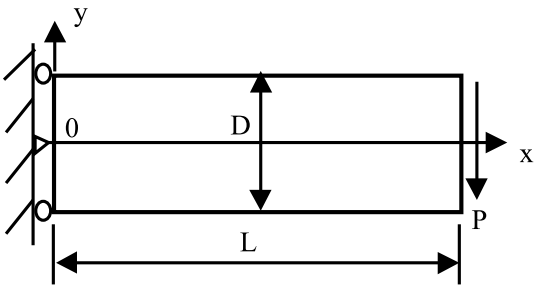

Fig. 3. A cantilever beam.

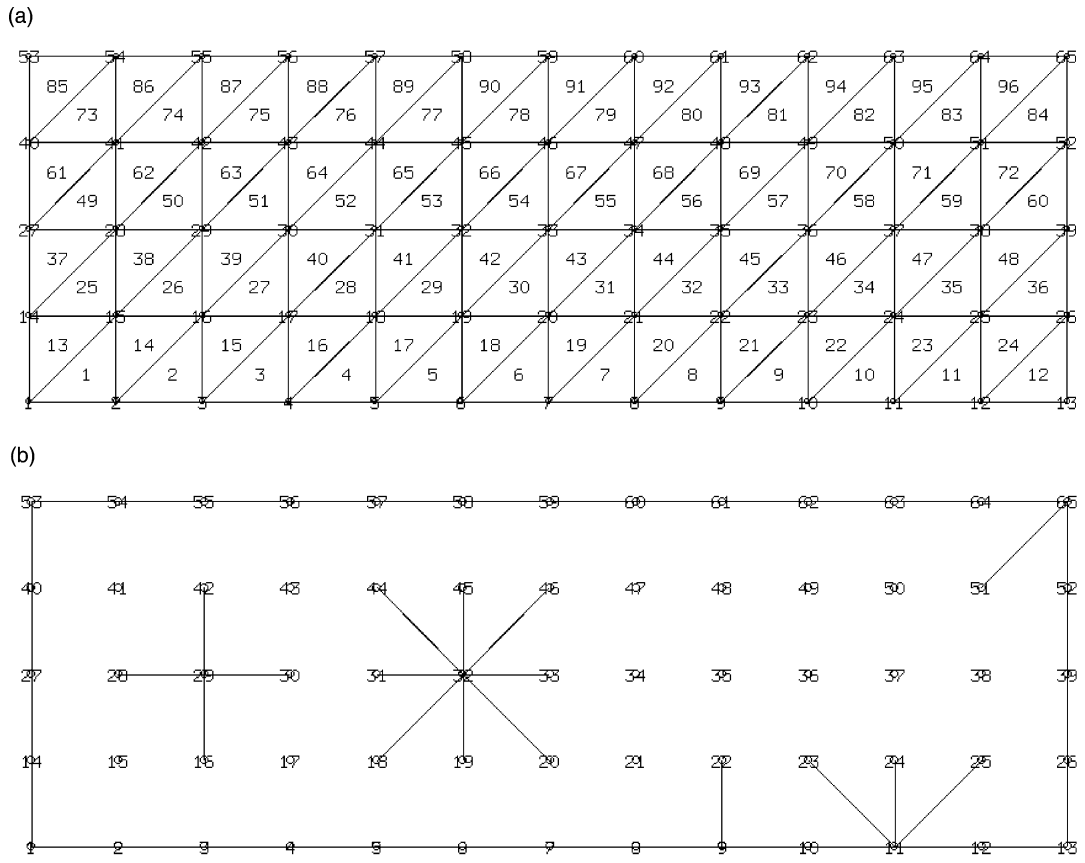

Fig. 4. (a) A FEM mesh with triangular elements and (b) point distribution for the PAM analysis.

where A_I is the total area of the palm (surrounding triangles) of point I, and A_Ω is the area of the whole problem domain.

$$\alpha_I^{\Gamma_u} = \frac{L_I}{\sum_{i=1}^{N_t} L_i} L_{\Gamma_u} \tag{16}$$

where L_I is the total length of the natural boundary on the two sides of point I, and L_{Γ_u} is the length of the whole natural boundary of the problem domain. There are some other means to calculate these coefficients (see Beissel et al., 1996). The conditions are that the summation of all the α_I^Ω for all the points must be the area of the problem domain, and that the summation of all the $\alpha_I^{\Gamma_u}$ for all the natural boundary points must be the total length of the natural boundary of the problem domain.

It should be mentioned here that the integration within a palm is carried out exactly as the integrand $\mathbf{B}^T\mathbf{D}\mathbf{B}$ is a constant for a triangle in the palm. Therefore, the stability problem associated with the nodal integration method (Beissel et al., 1996) does not exist in the present method. An example will be presented in Section 5 to illustrate this issue in detail. It may be also mentioned here that the approximately equal in Eqs. (13) and (14) can be changed to equal if an algorithm can be designed in such a manner that the overlapping area is evenly distributed over the problem domain.

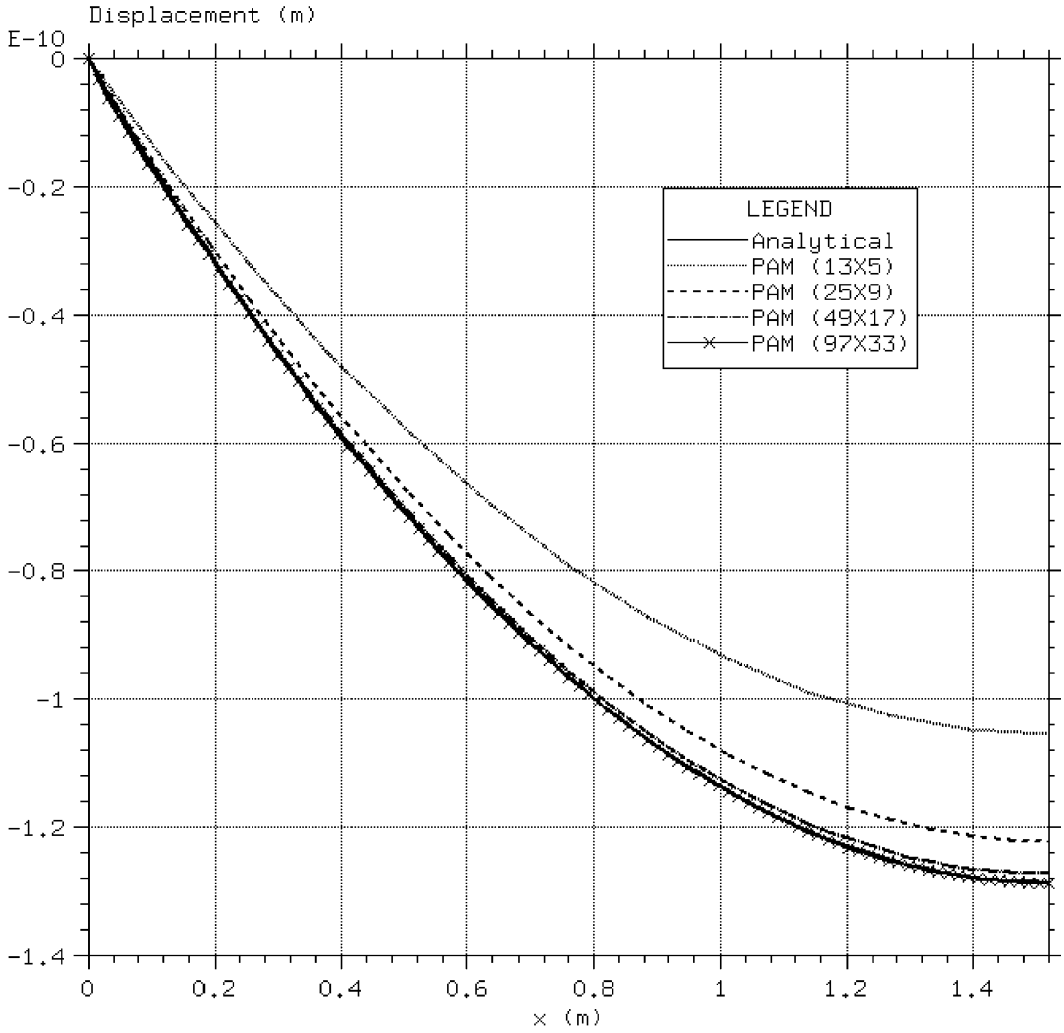

Fig. 5. Convergence of displacement u_x at $y = -D/2$.

4. Procedure of point assembly method

The PAM is coded in FORTRAN. The procedure of the program is summarized as follows:

1. Discretize the problem domain and its boundary by scattered points. This can be done using any post-processor for FEM codes.
2. Optimize the numbering of the points according to the equation solver. For example, if a half-bandwidth method is used in the solver, minimize the half-bandwidth.
3. Loop over all the points in the problem domain $\mathscr{P}$.
   (a) For a given point I, search for all the points within the circle of diameter d_g, and choose the surrounding points to form a palm.
   (b) Form the matrix of shape functions **N** for the palm and calculate **B** matrix.

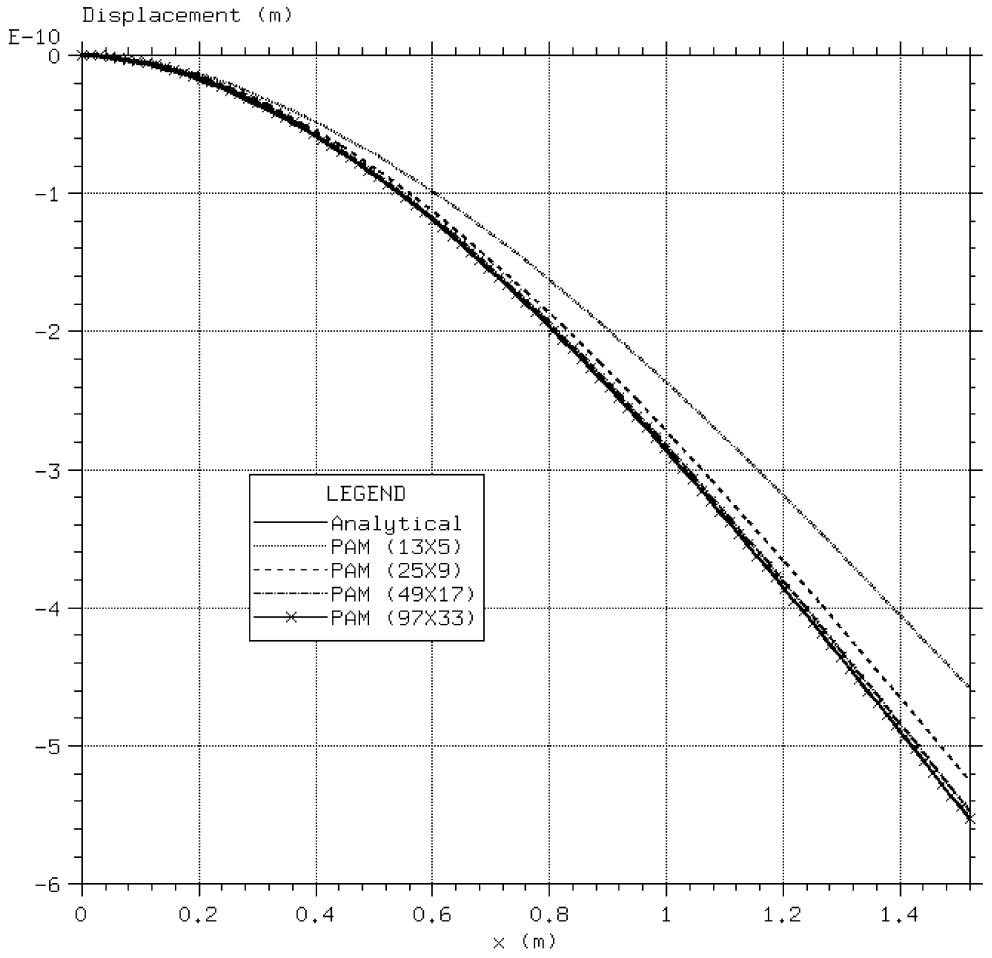

Fig. 6. Convergence of displacement u_y at $y = 0$.

(c) Calculate $\mathbf{B}^{\mathrm{T}}\mathbf{D}\mathbf{B}$ and assemble it to all the points covered by the palm, using Eqs. (13) and (14).
4. End the loop for all the points, and the globe stiffness matrix is formed.
5. Solve Eq. (9) for the displacements at all the points.
6. Calculate the strain and stress at desired points by forming palms for the points.

Most of the above procedures are very much similar to those in the FEM, except an algorithm is needed to form the palm. The best algorithms are such that ensure an even overlapping in area in the point assembly process, so that the approximately equal in Eqs. (13) and (14) can be replaced by an equal. An algorithm that cannot ensure an even area overlapping will result in an approximated stiffness matrix, and therefore an approximation in the results. Such an algorithm may not be able to pass the patch test, but always give an approximated solution for the problem. An algorithm has been developed for forming palm automatically. The program detects automatically if the overlapping is not even. The effectiveness of the algorithm is examined in the following section.

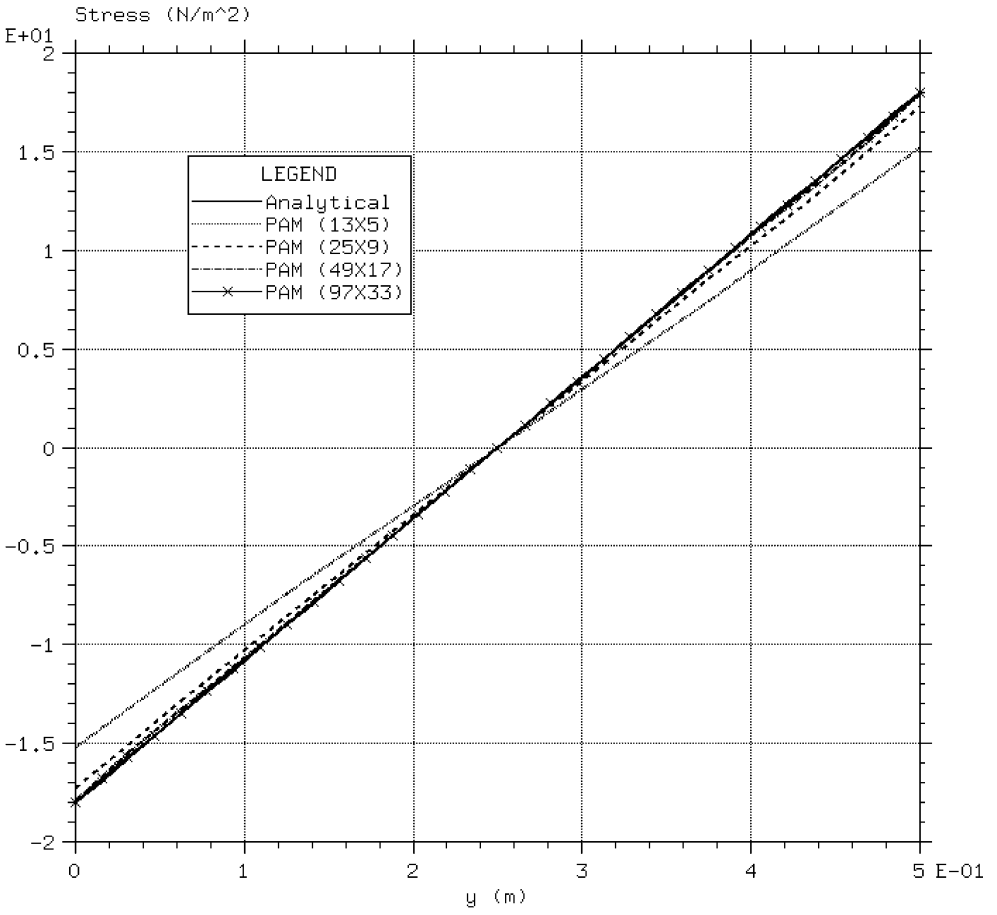

Fig. 7. Convergence of stress σ_{xx} at $x = L/2$.

5. Numerical results

5.1. Patch test

The first numerical example is the standard patch test, shown in Fig. 2. In these patch tests, the displacements are prescribed on all the outside boundaries of the patch as

$$\bar{\mathbf{u}} = \begin{Bmatrix} x \\ y \end{Bmatrix} \tag{17}$$

Satisfaction of the patch test requires that the displacements of any interior point be given by the same linear function and that the strain and stresses be constant in the patch.

The present PAM program passes the patch tests exactly for the patches with regularly distributed points (Fig. 2a), as well as irregularly distributed points (Fig. 2b). The strain and stress obtained in these two patches were constants.

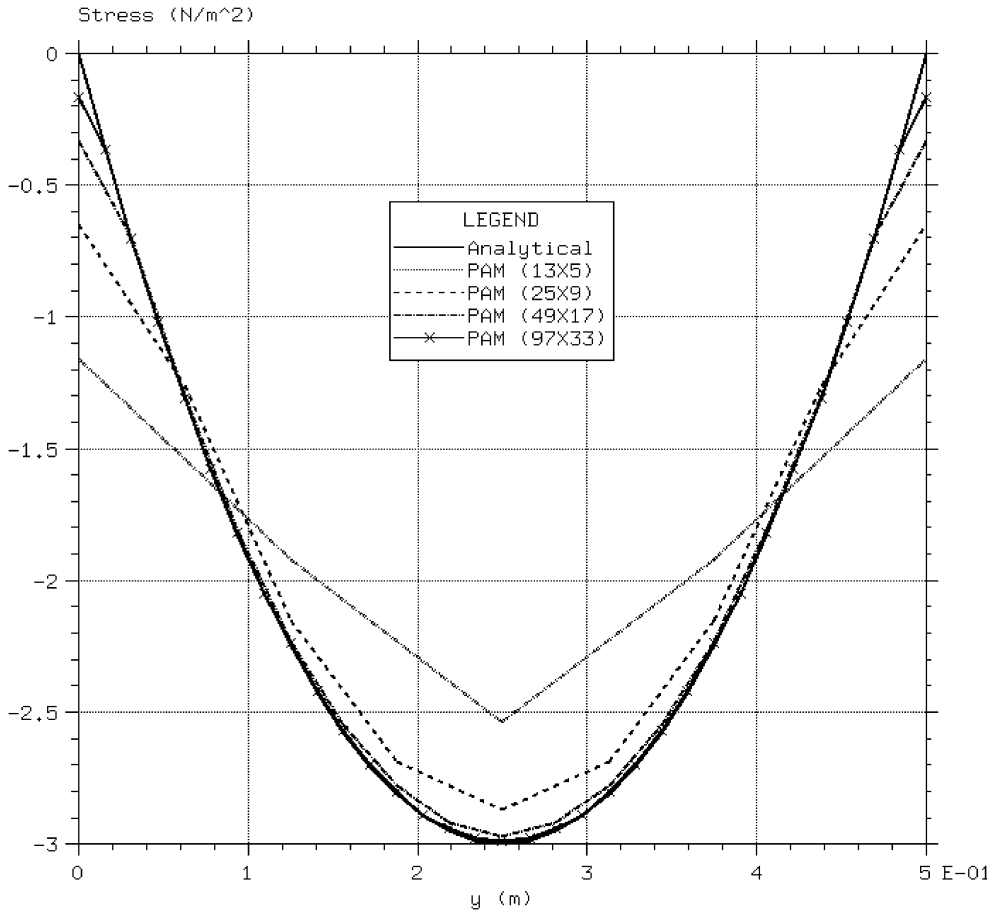

Fig. 8. Convergence of stress σ_{xy} at $x = L/2$.

5.2. Cantilever beam

Consider a cantilever beam of characteristic length L and height D subjected to a parabolic traction at the free end as shown in Fig. 3. The thickness of the cantilever is considered to be one unit, and is assumed to be in a state of plane stress.

The exact solution can be given by Timoshenko and Goodier (1970):

$$u_x = -\frac{Py}{6EI}\left[(6L - 3x)x + (2 + v)\left(y^2 - \frac{D^2}{4}\right)\right] \tag{18}$$

$$u_y = \frac{P}{6EI}\left[3vy^2(L - x) + (4 + 5v)\frac{D^2x}{4} + (3L - x)x^2\right] \tag{19}$$

where the moment of inertia I of the beam is given by

$$I = \frac{D^3}{12} \tag{20}$$

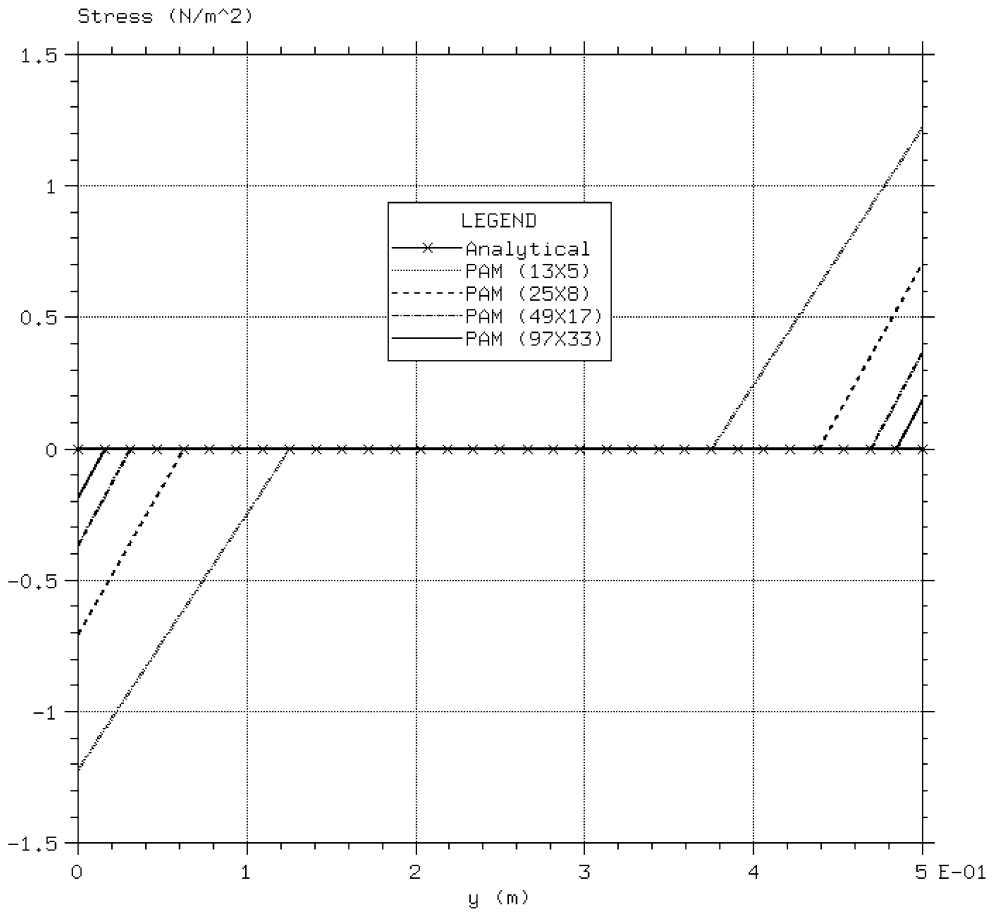

Fig. 9. Convergence of stress σ_{yy} at $x = L/2$.

The stresses corresponding to the displacements (18) and (19) are

$$\sigma_x(x,y) = -\frac{P(L-x)y}{I} \tag{21}$$

$$\sigma_y(x,y) = 0 \tag{22}$$

$$\sigma_{xy}(x,y) = -\frac{Py}{2I}\left(\frac{D^2}{4} - y^2\right) \tag{23}$$

In the following numerical examples, the parameters are taken as $E = 210$ GPa, $v = 0.3$, $D = 0.5$ m, $L = 1.5$ m, $P = 1$ N. Two methods, FEM and PAM are used in the numerical calculation. Fig. 4a shows the mesh configuration for the FEM calculation with a node density of 13×5, and Fig. 4b shows the points configuration for the PAM calculation with a point density of 13×5. In the PAM, the influence diameter is set to be $d_g = a$, where a is the length of the horizontal distance between the two adjacent points. This means that for an internal point, four surrounding points are employed (e.g., point 29 in Fig. 4b). For a

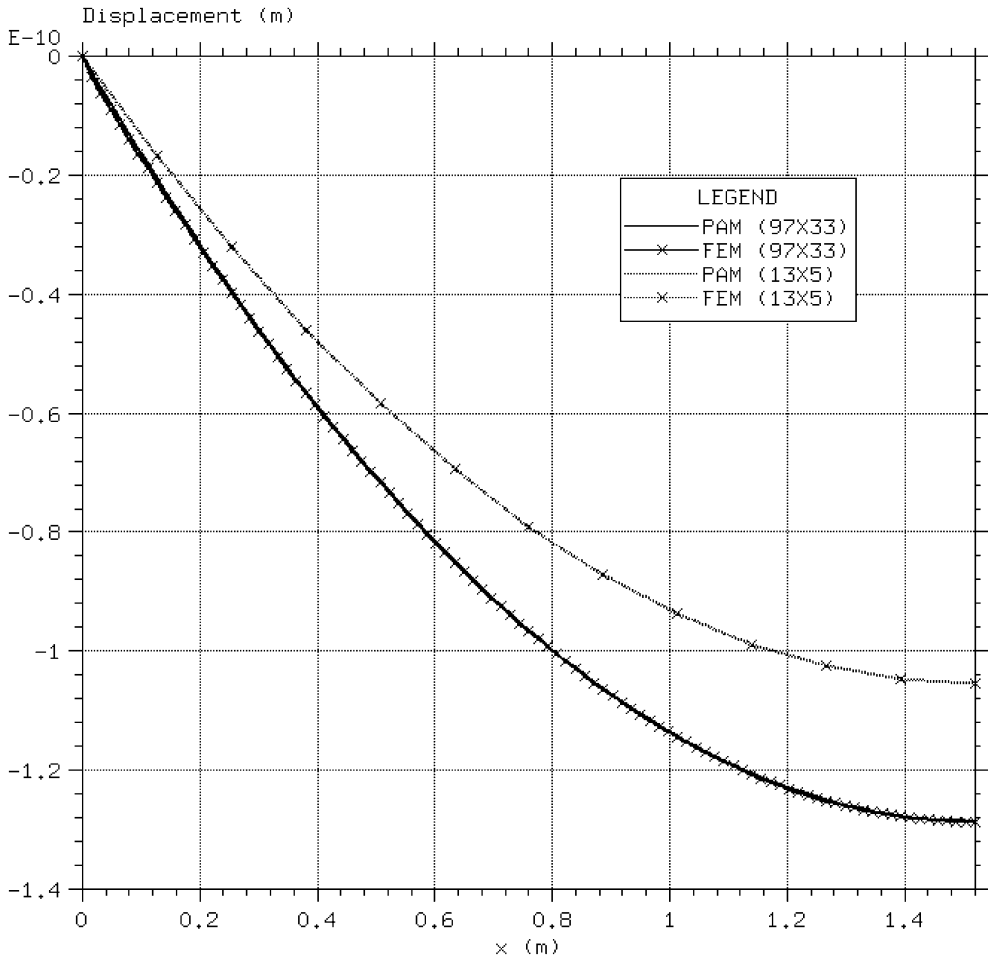

Fig. 10. Comparison of displacement u_x at $y = -D/2$ obtained by PAM and FEM.

point on the boundary, one internal and two boundary points, and for a point at the corner, two boundary points are employed (e.g., point 9 and point 1 in Fig. 4b).

Fig. 5 depicts the distribution of the displacement in the x-direction on the bottom surface of the beam ($y = -D/2$). The results are obtained by the analytical formulae and the PAM with different point densities. It is shown that the PAM results converge to the analytical solutions, and the PAM results with a density of 97×33 coincide with the analytical solution. Fig. 6 shows the distribution of the displacement in the y-direction. The results shown in Fig. 6 further confirm the conclusions drawn from Fig. 5.

Fig. 7 shows the distribution of the normal stress σ_{xx} on the cross-section at $x = L/2$. Very good agreement between the PAM results and the analytical results is shown even for the case of point density of 49×17. Fig. 8 depicts the distribution of the shear stress σ_{xy} on the cross-section at $x = L/2$. Very good agreement between the PAM results and the analytical results is shown even for the case of point density of 49×17, except on the two surfaces where the shear stress should be zero. The PAM results obtained using 97×33 can improve the results but disagreement on the surfaces persists. The similar situation can be observed from Fig. 9 for the distribution of stress σ_{yy}.

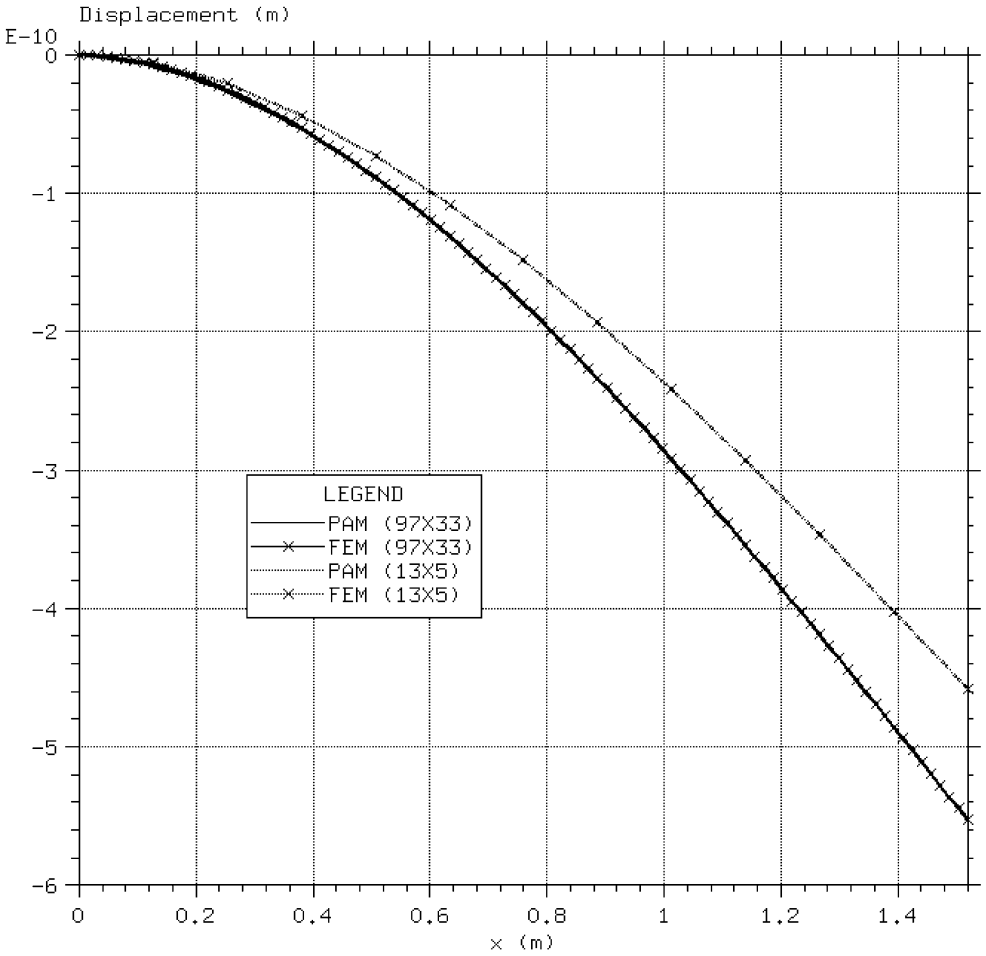

Fig. 11. Comparison of displacement u_y at $y = 0$ obtained by PAM and FEM.

Comparing the results with the results obtained by PAM and FEM, it is found that the accuracy on the displacement obtained by two methods are the same for the same density of points used, as shown in Figs. 10 and 11. The stress obtained by the PAM are slightly better than that of FEM, when $d_g = a$ is used for the PAM. However, in PAM, we have a freedom to choose a larger d_g, which means more points can be employed for point assembly and the stress–strain calculation. When $d_g = 1.415a$ is used instead of $d_g = a$, there are eight surrounding points for an internal point, five for a point on the boundary and three for a point at the corner (e.g., point 32, point 11, and point 5 in Fig. 4b). Fig. 12 shows the signification improvement on stress σ_{yy}, where $d_g = 1.415a$ is used. It is seen that the results are much more accurate than those obtained by FEM. It is, therefore, concluded that the PAM can produce more accurate results for stresses.

The point integration method has a problem with stability (Beissel et al., 1996), and a stabilization term is needed in the week form. The stability problem is resulted from insufficient integral points, which can be evidenced from the oscillation of stress distribution obtained using irregular nodes distribution. Although the idea of point integration method is employed in the present method, the stability problem does not

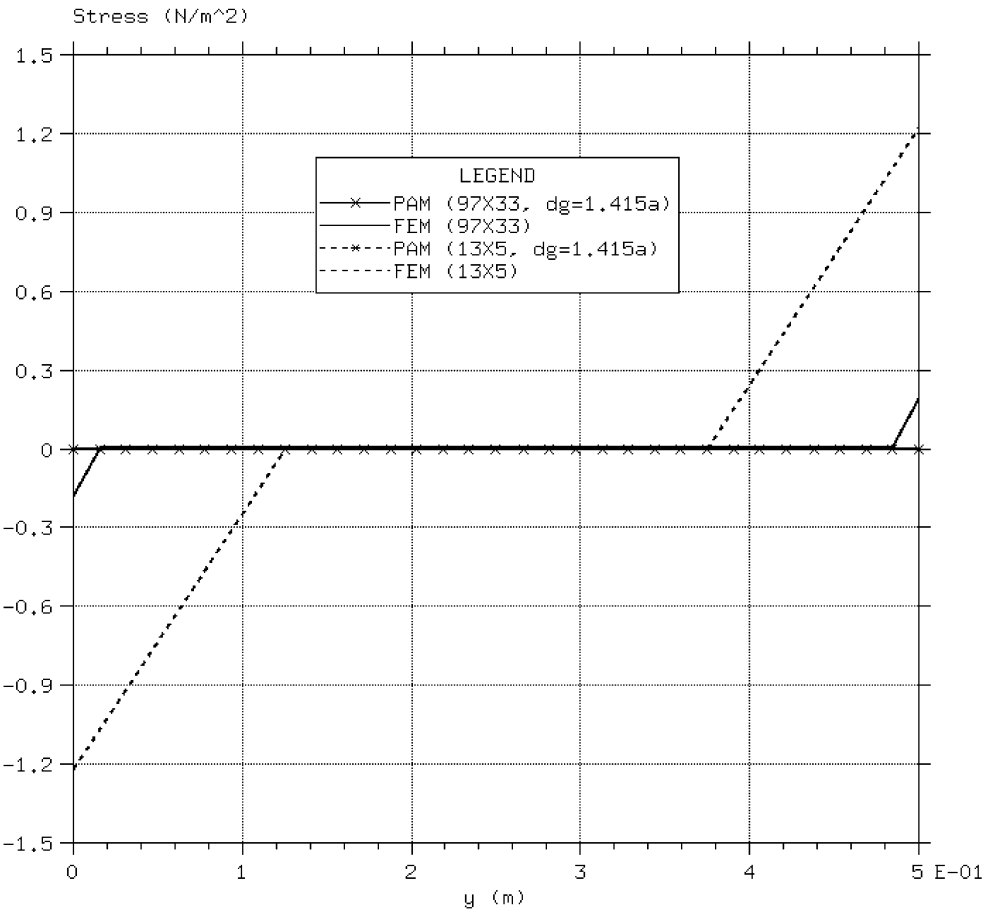

Fig. 12. Comparison of stress σ_{yy} at $x = L/2$ obtained by PAM and FEM.

exist. This is because the integration of the stiffness matrix for a palm can be carried exactly, as the integrand in the triangles of the palm is constant. This has already been seen in the patch test using irregularly distributed pints (Fig. 2b). To further confirm this, irregularly distributed points are used to compute the stress distribution in the cantilever beam. The irregular mesh has been generated by randomly moving the internal points in the regular mesh by up to 20% of the rib length of the palm in a random direction. For an easy comparison, the points at the cross-section $x = L/2$ is kept unmoved. The results for the share stress distribution at $x = L/2$ is plotted in Fig. 13 together with the analytical results and the results obtained using regularly distributed points. No oscillation is observed, and the results obtained using regular and irregular points are nearly indistinguishable from this figure.

As for the computation time, the time needed for the PAM to assemble the global stiffness matrix is about 2–3 times of that needed for the FEM, depends on d_g used in the PAM. However, for most of the problem, the CPU time used for solving the system equation dominates the total CPU time, and the stiffness matrix size is almost the same for both methods. Therefore, the PAM is nearly equally efficient as the FEM. For a problem with point density of 97×33 (6402 degree of freedoms in total), the CPU time required by PAM is about 4% more that by the FEM.

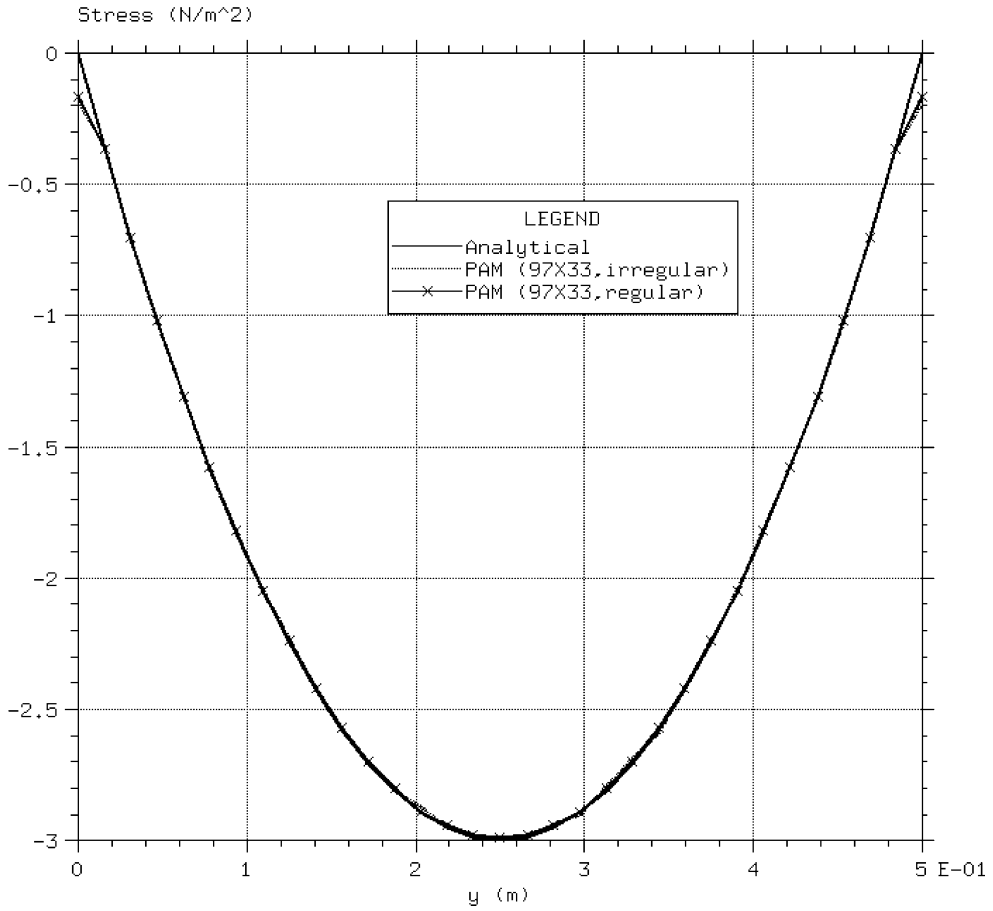

Fig. 13. Convergence of stress σ_{xy} at $x = L/2$. Comparison of the results obtained using regular and irregular meshes.

6. Conclusion

A novel PAM is presented for stress analysis for solids. Two-dimensional problems are considered in this work. The PAM makes good use of the effective techniques developed over half a century in the conventional FEM without dividing the problem domain into elements. A PAM program with an automatic point-searching algorithm has been developed in FORTRAN. Examples have been presented to demonstrate the efficiency of the PAM. The study has drawn the following conclusions:

1. The PAM is an entirely point based method. A mesh of element is totally unnecessary, and a background mesh for integration is also unnecessary.
2. The PAM is nearly equally efficient as the FEM. For a problem with 6402 degree of freedoms, the CPU time required by PAM is about 4% more that by the FEM.
3. The accuracy of the displacement obtained by the PAM is equivalent to that by the FEM using triangular elements with the same point density.
4. The accuracy of the strain/stress obtained by the PAM is more accurate than that of the FEM using triangular elements.

The present method has, unfortunately, drawbacks. The first drawback is that a very dense of points is needed to obtained accurate stresses. The present method cannot deal with incompressible elastic materials due to the volumetric locking. Special formulations, or different variational formulation are needed (see, e.g., Zienkiewicz and Taylor, 1989) to solve this problem. These two drawbacks are inherited from the conventional triangular finite elements. The third drawback is the difficulty to develop a comprehensive algorithm to ensure an even overlapping of integration, especially when the irregularity of the point distribution is severe. An indication on whether the overlapping is even or not can be easily outputted for checking. When the overlapping is not even, the results obtained are an approximation, and the controlling of the accuracy needs to be further investigated.

References

Beissel, S., Belytschko, T., 1996. Nodal integration of the element-free Galerkin method. Comput. Meth. Appl. Mech. Engng. 139, 49–74.

Belytschko, T., Gu, L., Lu, Y.Y., 1994a. Fracture and crack growth by element free Galerkin methods. Model. Simul. Mater. Sci. Engng. 2, 519–534.

Belytschko, T., Lu, Y.Y., Gu, L., 1994b. Element-free Galerkin methods. Int. J. Numer. Meth. Engng. 37, 229–256.

Belytschko, T., Lu, Y.Y., Gu, L., 1995a. Crack propagation by element-free Galerkin methods. Engng. Frac. Mech. 51, 295–315.

Belytschko, T., Lu, Y.Y., Gu, L., Tabbara, M., 1995b. Element-free Galerkin methods for static and dynamic fracture. Int. J. Solids Struct. 32, 2547–2570.

Belytschko, T., Krongauz, Y., Organ, D., Fleming, M., Krysl, P., 1996a. Meshless methods: an overview and recent developments. Comput. Meth. Appl. Mech. Engng. 139, 3–47.

Belytschko, T., Tabbara, M., 1996b. Dynamic fracture using element-free Galerkin methods. Int. J. Numer. Meth. Engng. 39, 923–938.

Duarte, A.C., Oden, J.T., 1995. Hp clouds—a meshless method to solve boundary-value problems, TICAM report 95–05, 1995.

Gingold, R.A., Moraghan, J.J., 1977. Smoothed particle hydrodynamics: theory and applications to non spherical stars. Man. Not. Roy. Astron. Soc. 181, 375–389.

Gosz, J., Liu, W.K., 1996. Admissible approximations for essential boundary conditions in the reproducing kernel particle method. Computat. Mech. 19, 120–135.

Günther, F.C., Liu, W.K., 1998. Implementation of boundary conditions for meshless methods. Comput. Meth. Appl. Mech. Engng. 163 (1–4), 205–230.

Krysl, P., Belytschko, T., 1995. Analysis of thin plates by the element-free Galerkin methods. Comput. Mech. 17, 26–35.

Liu, G.R., Yang, K.Y., 1998. In: A penalty method for enforcing essential boundary conditions in element free Galerkin method. Proceedings of the Second HPC Asia'98, Singapore, pp. 715–721.

Liu, W.K., Chen, Y., 1995. Wavelet and multiple scale reproducing kernel particle methods. Int. J. Numer. Meth. Fluids. 21, 901–931.

Liu, W.K., Chen, Y., Jun, S., Chen, J.-S., Belytschko, T., Pan, C., Uras, R.-A., Chang, C.-T., 1996. Overview and applications of the reproducing kernel particle methods. Arch. Comput. Meth. Engng.: State Art Rev. 3, 3–80.

Liu, W.K., Jun, S., Li, S., Adee, J., Belytschko, T., 1995a. Reproducing kernel particle methods for structural dynamics. Int. J. Numer. Meth. Engng. 38, 1655–1679.

Liu, W.K., Jun, S., Zhang, Y., 1995b. Reproducing kernel particle methods. Int. J. Numer. Meth. Fluid. 20, 1081–1106.

Lu, Y.Y., Belytschko, T., Gu, L., 1994. A new implementation of the element-free Galerkin method. Comput. Meth. Appl. Mech. Engng. 113, 397–414.

Moraghan, J.J., 1982. Why particles methods work, SIAM. J. Sci. Statist. Comput. 3, 422–433.

Moraghan, J.J., 1988. An introduction to SPH. Comput. Phys. Commun. 48, 89–96.

Nayroles, B., Touzot, G., Villon, P., 1992. Generalizing the finite element method: Diffuse approximation and diffuse elements. Comput. Mech. 10, 307–318.

Oqate, E., Idelsohn, S., Zienkiewicz, O.C., Fisher, T., 1995. In: A finite point method for analysis of fluid flow problems. Proceedings of nineth International Conference on Finite Element Methods in Fluids, Venize, Italy, pp. 15–21.

Oqate, E., Idelsohn, S., Zienkiewicz, O.C., Taylor, R.L., 1996. A finite point method in computational mechanics. Applications to convective transport and fluid flow. Int. J. Numer. Meth. Engng. 39, 3839–3866.

Timoshenko, S.P., Goodier, J.N., 1970. Theory of Elasticity, third ed. McGraw-Hill, New York.

Zienkiewicz, O.C., Taylor, R.L., 1989. The finite element method, fourth ed. McGraw-Hill, New York.